

# Bandwidth-enhanced, Electrically Small, Planar, Endfire-radiating Huygens Dipole Antenna

Qingli Lin, *Student Member, IEEE*, Ming-Chun Tang, *Senior Member, IEEE*, Mei Li, *Member, IEEE*, Yunlu Duan, Zhehao Zhang, and Richard W. Ziolkowski, *Life Fellow, IEEE*

**Abstract**— A bandwidth-enhanced, electrically small, planar, endfire-radiating Huygens dipole antenna (HDA) is presented. The near-field resonant parasitic (NFRP) grid-shaped dipole and two concentric interdigitated capacitor (IDC) loaded loops enable broad electric and magnetic dipole responses, respectively. Benefiting from the additional capacitance introduced by the dual-loop design, the magnetic dipole response is achieved at a lower frequency. The consequent balanced resonant responses of the electric and magnetic NFRP elements yield a wideband and electrically small HDA with endfire-radiating performance characteristics. The fabricated prototype exhibited measured results that closely agree with their simulated values. Being an electrically small,  $ka = 0.91$ , system, it had an 8.79% fractional bandwidth and a 4.7 dBi peak realized gain. Furthermore, the antenna achieved unidirectional radiation patterns and maintained high radiation efficiency (RE),  $RE > 81\%$ , within its entire operational bandwidth.

**Index Terms**—Bandwidth-enhanced, electrically small antenna, endfire radiating, Huygens dipole antenna, near-field resonant parasitic (NFRP) element.

## I. INTRODUCTION

Wireless communications and sensor networks continue to advance at a rapid pace, the demands for compact sized equipment exhibiting enhanced radiation properties have increased dramatically. In particular, there is an intense need for the development of planar antennas with unidirectional performance characteristics that will facilitate various point-to-point applications associated with handheld devices and mobile terminals [1]-[3]. In recent years, there has been growing interest in electrically small Huygens dipole antennas (HDAs) because they have significant advantages for wireless applications. These advantages include compact sizes, high front-to-back ratios (FTBRs), wide beamwidths, and

independence of any ground plane [4]-[7]. As a result, HDAs have emerged as attractive candidates for various wireless applications. To date, numerous electrically small HDAs have been reported, incorporating near-field resonant parasitic (NFRP) elements to achieve the required balanced electric and magnetic responses for their unidirectional, cardioid performance characteristics. These designs include linearly polarized (LP) [8]-[10], circularly polarized [11] (CP), dual-LP [12], dual-CP [13], and pattern-/polarization-reconfigurable systems [14]-[16]. However, because of their electrically small size and consequent high Q-factors, many of these HDAs have narrow operating bandwidths. By integrating active elements such as non-Foster circuits [17] and varactor diodes [18] into the NFRP elements, the bandwidths of these antennas have been significantly improved. Nevertheless, the design complexities and costs introduced by those active circuits are generally an obvious disadvantage. Although bandwidth-enhanced Huygens antennas with fractional bandwidths (FBWs) of 6.1% [19] and 13.4% [20] were obtained using complementary configurations, they were not electrical small, i.e., their  $ka$  values at their lowest operational frequency were as high as 1.25 (i.e., an antenna is electrically small if  $ka = 2\pi a/\lambda < 1$ , where  $a$  represents the radius of the smallest sphere that completely encloses the entire antenna system, and  $\lambda$  refers to the free-space wavelength corresponding to its operating frequency). Consequently, it would be quite attractive to develop an innovative wideband, electrically small HDA.

A bandwidth-enhanced, electrically small, planar, endfire-radiating HDA is presented in this letter. The design is composed of two NFRP elements, i.e., a grid-shaped electric dipole and a specially designed dual-loop magnetic dipole, which exhibit broader electric and magnetic dipole frequency responses, respectively. Moreover, the coupling of the two loops introduces additional capacitance; their combination facilitates the overall system with an electrically small size. The optimized design balances the dipole responses of the electric and magnetic NFRP elements to realize an electrically small, wideband, endfire-radiating HDA. The fabricated and tested prototype demonstrated its  $ka = 0.91$  at its lowest operational frequency, an 8.79% FBW, a 4.7 dBi peak realized gain (RG), and a high radiation efficiency (RE) over its entire bandwidth. With its exceptional performance characteristics, this HDA is an extremely attractive option for a wide range of space-limited wireless communications and sensor network applications.

Manuscript received on July 18, 2023; revised on October 05, 2023, and accepted on November 09, 2023.

This work was supported by the National Natural Science Foundation of China grant number 62031006, in part by the Natural Science Foundation of Chongqing under contract number CSTB2022NSCQ-MSX0597, and in part by the Venture & Innovation Support Program for Chongqing Overseas Returnees under contract number cx2022063. (*Corresponding author: Ming-chun Tang.*)

Q. Lin, M. -C. Tang, M. Li, Y. Duan, and Z. Zhang are with the Key Laboratory of Dependable Service Computing in Cyber Physical Society Ministry of Education, School of Microelectronics and Communication Engineering, Chongqing University, Chongqing 400044, China (e-mail: tangmingchun@cqu.edu.cn);

R. W. Ziolkowski is with the Department of Electrical and Computer Engineering, University of Arizona, Tucson, AZ 85721 USA (e-mail: ziolkowski@ece.arizona.edu).

## II. ANTENNA DESIGN AND MAIN OPERATING FEATURES

The configuration and design parameters of the developed bandwidth-enhanced electrically small HDA are shown in Fig. 1. It consists of two concentric interdigitated capacitor (IDC) loaded loops, a grid-shaped dipole, and a driven dipole. They are printed on two copper-clad dielectric substrates, designated as Layer\_1 and Layer\_2. Both substrates are Rogers 4003C material which has a relative dielectric constant ( $\epsilon_r$ ) of 3.38, a loss tangent ( $\tan \delta$ ) of 0.0027, and a copper thickness of 0.017 mm. The radius of the substrates is  $R_1 = 25.0$  mm. Layer\_1 has a thickness of  $H_1 = 0.508$  mm, and Layer\_2 has a thickness of  $H_2 = 0.203$  mm.

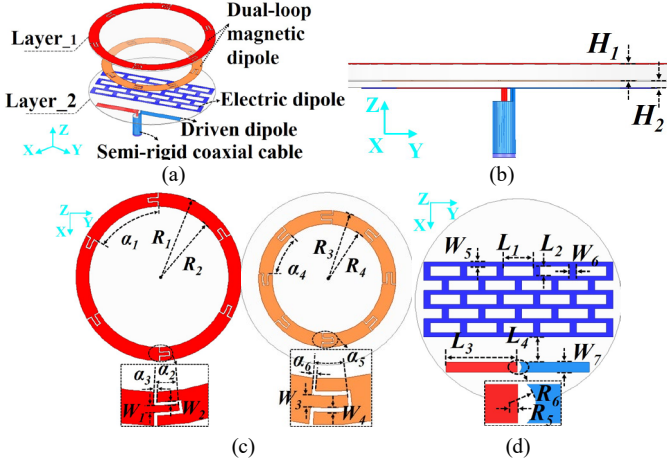


Fig. 1. Configuration of the developed bandwidth-enhanced, electrically small, planar, endfire-radiating HDA. (a) Three-dimensional view. (b) Side view. (c) Top and bottom view of the concentric IDC-loaded loops. (d) Top view of the grid-shaped electrical dipole and the driven dipole. The detailed design parameters (in mm):  $H_1 = 0.508$ ,  $H_2 = 0.203$ ,  $L_1 = 7.24$ ,  $L_2 = 2.4$ ,  $L_3 = 17.17$ ,  $L_4 = 6.2$ ,  $W_1 = 0.8$ ,  $W_2 = 0.4$ ,  $W_3 = 1.0$ ,  $W_4 = 0.4$ ,  $W_5 = 1.05$ ,  $W_6 = 1.6$ ,  $W_7 = 2.4$ ,  $R_1 = 25$ ,  $R_2 = 21$ ,  $R_3 = 19.8$ ,  $R_4 = 15.9$ ,  $R_5 = 0.47$ ,  $R_6 = 1.57$ ,  $\alpha_1 = 60^\circ$ ,  $\alpha_2 = 7.5^\circ$ ,  $\alpha_3 = 1^\circ$ ,  $\alpha_4 = 45^\circ$ ,  $\alpha_5 = 10^\circ$ , and  $\alpha_6 = 1^\circ$ .

Fig. 1(c) provides a detailed illustration of the design parameters for the concentric IDC-loaded loops. The outer loop is comprised of six equally spaced coupling lines, each being interlaced to its adjacent neighbor by an IDC. The outer radius is denoted as  $R_1$ ; the inner radius is represented as  $R_2$ . The angle subtending each of the IDC-interlaced coupling lines is  $\alpha_1 = 60^\circ$ . The detailed parameters of each IDC in the outer loop are: its inner metal stub has the width  $W_1$ ; each air stub has the inner width  $W_2$ ; the angle  $\alpha_2$  defines the air gap of the IDC; and  $\alpha_3$  is the angle between the start of an IDC and its termination. The inner IDC-loaded loop, whose outer and inner radii are  $R_3$  and  $R_4$ , respectively, is divided into eight equal-length segments connected with IDCs in the same manner as the outer loop. The angle subtended by each of these coupling lines is  $\alpha_4 = 45^\circ$ . The detailed parameters of each IDC of the inner loop are: its inner metal stub has the width  $W_3$ ; each air stub has the inner width  $W_4$ ; the angle  $\alpha_6$  defines the air gap of the IDC; and  $\alpha_5$  is the angle between the start of an IDC and its termination.

Fig. 1(d) illustrates the design parameters for both the grid-shaped electrical dipole and the driven dipole. The grid electric dipole consists of 23 rectangular cells that have the same dimensions but are staggered by a half-cell in each neighboring row. The middle line is composed of five cells and

its center coincides with the centers of the substrates. The grid cells are characterized by a longer side, denoted as  $L_1$ , and a shorter side, denoted as  $L_2$ , with corresponding widths of  $W_5$  and  $W_6$ , respectively. The driven dipole is positioned at a distance  $L_4$  from the bottom edge of the grid array structure. Its two arms have the same dimensions, i.e., length  $L_3$  and width  $W_7$ .

### A. IDC-based dual-loop acts as a miniaturized broadband magnetic dipole

Fig. 2(a) presents four magnetic-based NFRP loop antennas. Their simulated reflection coefficients ( $|S_{11}|$ ) and 3-D radiation patterns at each resonance frequency point are given in Fig. 2(b). Notably, the simple gap-loop antenna has antipodal slots etched on its single loop. It resonates at  $f_{\text{res}} = 1.64$  GHz and exhibits a narrow -10-dB impedance FBW of only 1.8%. Benefitting from the broadband magnetic response of its IDC-loaded loop [21], the slightly larger 6 IDC-based single loop antenna exhibits a broader FBW of 4.8%, but  $f_{\text{res}}$  becomes higher at 2.05 GHz. Even more IDCs in the loop would lead to an even more uniform aperture field and a less out-of-roundness  $xOy$ -plane pattern. However, they would effectively decrease the overall capacitance, i.e., the IDCs in the loop are capacitances in series and, hence, they would lead to an even higher  $f_{\text{res}}$ . Therefore, a smaller periodic IDC-loaded loop is introduced concentrically with the larger one. This arrangement increases the overall capacitance, i.e., the loops act in parallel and the gap between them introduces yet more capacitance. The final dual IDC-loop antenna design achieves a much lower  $f_{\text{res}} = 1.66$  GHz with its  $\text{FBW} = 3.5\%$ . Consequently, the overall electrical size is reduced as well. Thus, the main contributions of the dual-loop configuration are to obtain a wideband magnetic dipole mode and a reduced electrical size of the entire system.

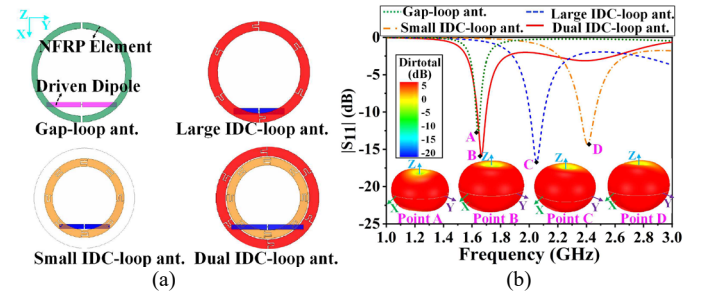


Fig. 2. Four magnetic-based NFRP loop antennas. (a) Configurations. (b) Simulated  $|S_{11}|$  values and the three-dimensional radiation patterns at their resonance frequencies.

### B. Grid array acts as a broadband electric dipole

In accordance with the theory of Huygens sources, a well-balanced combination of an electric dipole and an orthogonal, in-phase magnetic dipole will result in unidirectional radiation pattern [22]. In previous HDA designs [5], [6], strip dipoles were utilized to act as the electric dipoles. Innovatively, a single-layer inductive-grid array structure is adopted herein to serve as the requisite broadband orthogonal electric dipole. As was demonstrated in our previous work [23], it effectively generates a fundamental electric mode with broader bandwidth than that of a simple electric dipole.

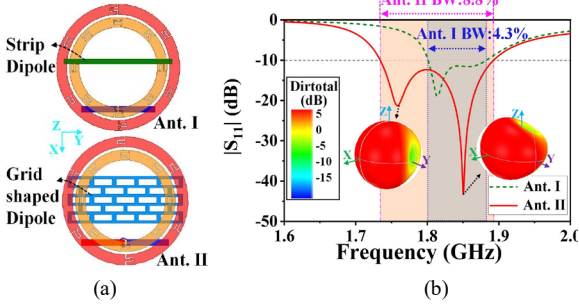


Fig. 3. Comparison of the reference and the developed bandwidth enhanced, electrically small, endfire HDA. (a) Configurations. (b)  $|S_{11}|$  values.

To illustrate the broadband performance of the grid-shaped electric dipole, a comparison between HDAs with a grid-shaped dipole and a strip-shaped dipole is depicted in Fig. 3(a). The reference HDA with a strip-shaped electric dipole, i.e., Ant. I, yields a FBW = 4.3%, ranging from 1.80 to 1.88 GHz, with  $ka = 0.94$ . In contrast, the developed HDA, Ant. II, with its grid-shaped electric dipole yields a much broader bandwidth with FBW = 8.8%, ranging from 1.73 to 1.89 GHz, with  $ka = 0.90$ , i.e., the FBW is more than doubled even with a smaller electrical size. Being printed on its dielectric substrate, the grid array's long side length is selected to be approximately equivalent to half the wavelength of its fundamental resonance and is selected by design so that it occurs near the magnetic dipole's. As also shown in Fig. 3(b), the three-dimensional directivity patterns at the resonance frequency points of Ant. II are unidirectional. These results confirm the pivotal role of the grid array structure in broadening the overall bandwidth of the developed HDA. It effectively acts as a broadband electric dipole that is balanced with the magnetic one component.

Moreover, the grid array also serves as an inductive impedance surface that loads the concentric IDC-loaded loops. Since the characteristic impedance of the grid array is intrinsically linked to the unit cell size and number, the magnetic dipole's resonance location can be finely tuned through modification of the grid parameters. Specifically, the grid's unit cell size basically determines its resonance frequency. The length of the grid and the number and arrangement of its unit cells control its inductance. It is possible for the electric and magnetic resonances to coincide closely by optimizing those parameters. This process enhances not only its impedance bandwidth, but also its unidirectional performance, i.e., its FTBR values over that bandwidth.

### C) Surface current distributions

Fig. 4 shows the surface current distributions to illustrate the endfire radiating mechanisms of the developed wideband, electrically small HDA. It is observed that the currents on the grid-shaped dipole are primarily directed along the  $y$ -axis near  $T/4$  and  $3T/4$ . At times 0 and  $T/2$ , relatively uniform loop current distributions are formed by the dual-loop dipole. Hence, a phase difference of  $90^\circ$  exists between the electric dipole and magnetic dipole. It is well-known that the expression for the equivalent magnetic current moment of a small current loop, driven by a constant current  $I_0$ , is  $I_m = j\omega\mu_0 I_0 A/L$ , where  $A$  is the area of the loop and  $L$  is its inductance [24]. Consequently,

the phase of the equivalent magnetic dipole leads the actual loop current by  $90^\circ$ . This implies that the current moments of the grid-shaped electric dipole and the dual-loop magnetic dipole resonate in-phase, enabling the desired attainment of a unidirectional cardioid pattern [25].

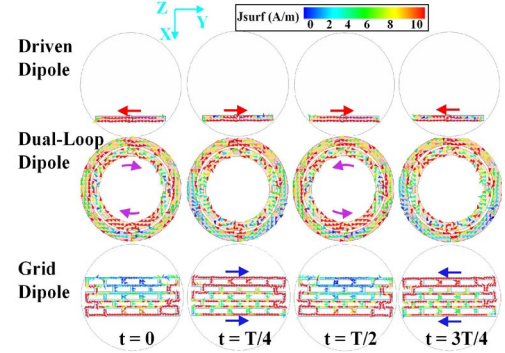


Fig. 4. Surface current distributions on the driven dipole, dual-loop dipole, and grid dipole at quarter period intervals at 1.8 GHz.

### III. SIMULATED AND MEASURED RESULTS

The optimized HDA design was manufactured, assembled, and tested. To enhance the accuracy of the measurements, a sleeve balun having a length of 40.0 mm and a radius of 3.0 mm was incorporated into the measurement procedure. Typically, a sleeve balun can attain a 10% relative bandwidth [26]. Its inclusion was necessary to minimize the negative effects caused by spurious currents induced on the outer walls of the lengthy coaxial cable associated with the measurement system [26]. Fig. 5(a) displays the fabricated layers and sleeve balun prior to assembly. Fig. 5(b) shows the assembled prototype attached to the sleeve balun. An Agilent E8361A vector network analyzer was used to measure the  $|S_{11}|$  values. The RG, radiation patterns, overall efficiency (OE), and FTBR values were obtained using an SG128 multiprobe antenna measurement system at the China Academy of Information and Communications Technology, Chongqing, China [27]. The antenna under test (AUT) within the measurement chamber is depicted in Fig. 5(c).

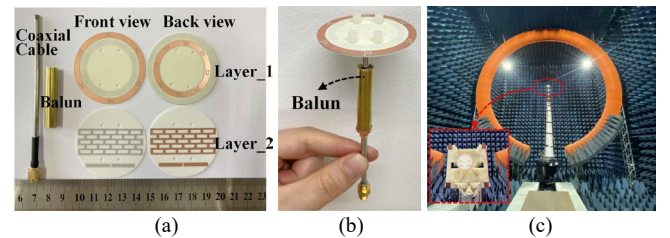


Fig. 5. Optimized HDA prototype. (a) Antenna's components before assembly. (b) Side view of the assembled antenna mounted on a sleeve balun. (c) AUT in the anechoic measurement chamber.

Fig. 6(a) presents the simulated and measured  $|S_{11}|$  and RG values of the prototype. The simulated (measured) -10-dB impedance bandwidth spans from 1.73 (1.74) to 1.89 (1.9) GHz, yielding an 8.8% (8.79%) FBW. The simulated (measured) electrical size of the prototype ranges from 0.90 (0.91) to 0.99 (0.99) across the lower to upper bounds of the FBW. The simulated (measured) RG values remained stable around 4.4 (4.0) dBi with a negligible gain fluctuation of only 0.5 (0.7) dB.

As shown in Fig. 6(b), the simulated (measured) OE values consistently exceeded 87% (81%) and the simulated (measured) FTBR values remained above 5.8 (5.5) dB throughout the entire FBW.

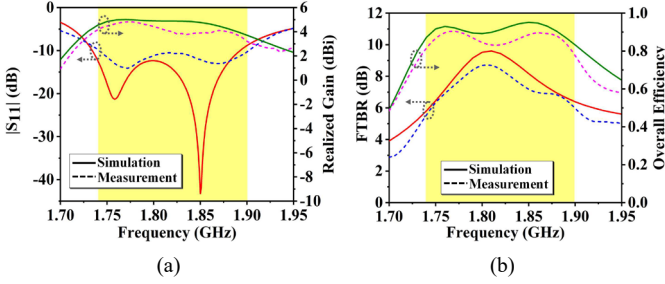


Fig. 6. Simulated and measured (a)  $|S_{11}|$  and RG, and (b) FTBR and OE values of the bandwidth-enhanced, electrically small, endfire-radiating HDA prototype as functions of the source frequency. The FBW is indicated by the yellow shading.

The simulated and measured normalized RG patterns have their maximum directed along the  $+x$ -axis at 1.81 GHz as shown in Fig. 7. These patterns confirm that it attained its predicted unidirectional endfire-radiating performance. Also note that its simulated (measured) cross-polarization levels along the  $+x$ -axis are below  $-37$  ( $-21$ ) dB. The observed difference between the simulated and measured results is acceptable because it arises mainly from fabrication tolerances and common experimental errors. Moreover, the antenna had to be mounted on a metal frame in the anechoic chamber because it lacked a ground plane. Since they were predicted to be extremely small, all of these issues inevitably led to the elevated measured cross-polarization values. Overall, there is a high degree of consistency between the measure results and their corresponding simulated values.

To emphasize the novel features and advantages of the developed antenna, Table I presents a comprehensive comparison with several recently reported unidirectional antennas. The developed antenna achieves a significantly wider bandwidth compared with the electrically small endfire radiating HDAs reported in [6], [7], [10], [11], and [15]. In contrast to the broadband endfire-radiating antennas reported in [19], the developed antenna achieves a broader FBW while maintaining a significantly smaller electrical size. The developed HDA possesses several valuable performance characteristics, including a wide bandwidth, small electrical size, effective endfire radiation, and acceptable FTBR. These features make the developed HDA an extremely appealing option for numerous spaced-limited wireless communication and sensor network applications such as emergency medical systems [28], [29]. Moreover, our simulation studies of a modest redesign, i.e.,  $L_1 = 6.94$ ,  $R_2 = 21.2$ ,  $R_3 = 18.6$ ,  $R_4 = 15.4$ ,  $L_4 = 6.4$  (in mm), show that by sacrificing some of the bandwidth, it could be readily modified for applications that require higher FTBR values. As noted in Table I, it remains electrically small with  $ka = 0.96$  and has a 4.2% overlapping FBW ( $|S_{11}| < -10$  dB and FTBR  $> 10$  dB) while exhibiting a 26.7 dB peak FTBR value. While its FBW is smaller than our prototype's, it is nevertheless larger than those of all the comparison examples.

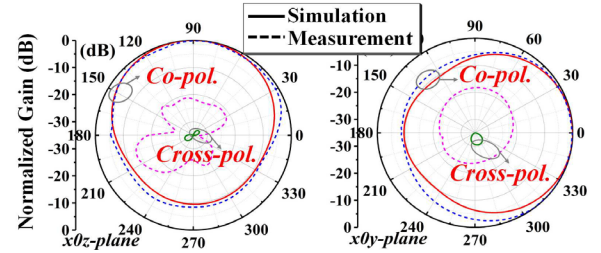


Fig. 7. The simulated and measured normalized RG patterns of the prototype at 1.81 GHz.

TABLE I  
PERFORMANCE COMPARISON OF THE DEVELOPED PROTOTYPE WITH  
RECENTLY REPORTED UNIDIRECTIONAL ANTENNAS

Refs.	Size( $\lambda_0^3$ )	$ka$	BW (%)	Peak RG (dBi)	Peak FTBR (dB)	OE (%)
[3]	$0.19 \times 0.38 \times 0.003$	1.69	1.1	1.9	20	61
[6]	$0.3 \times 0.079 \times 0.0015$	0.98	0.54	4.6	15	N.G.
[7]	$\pi \times (0.15)^2 \times 0.003$	0.98	0.5, 0.86	2.08, 2.48	13.6, 10.6	60
[10]	$\pi \times (0.07)^2 \times 0.009$	0.47	2.19	2.89	18	71
[11]	$0.287 \times 0.287 \times 0.048$	0.90	0.46	2.15	12	60
[15]	$\pi \times (0.15)^2 \times 0.0026$	0.98	2.38	5.4	13	85
[19]	$0.296 \times 0.296 \times 0.0067$	1.25	6.1	4.8	34	90
This work	$\pi \times (0.145)^2 \times 0.004$	0.91	8.79	4.7	8.7	81
Redesign	$\pi \times (0.15)^2 \times 0.004$	0.96	6.3	5.6	26.7	85

\* $\lambda_0$  and  $k$  are calculated at the lowest frequency of the FBW.

#### IV. CONCLUSION

A bandwidth-enhanced, electrically small, planar, endfire-radiating HDA was presented. It is composed of a driven dipole, a grid-shaped electric dipole element, and a specially-designed IDC-based dual-loop magnetic dipole element. The magnetic element achieved its broadband response through the arrangement of two concentric loops, each having periodic IDC loadings. Moreover, the mutual coupling of the two loops increased the overall capacitance, which decreased its resonance frequency. As a result, the entire antenna system was effectively reduced to an electrically small size. The balanced combination of this broadband magnetic dipole with the broadband grid-shaped electric dipole yielded the endfire-radiating HDA performance. The prototype of the developed HDA showed excellent agreement with its simulated values, achieving a 4.7 dBi peak RG with its RE  $> 81\%$  over its entire 8.79% FBW. Furthermore, the prototype demonstrated an electrically small size, with its  $ka$  values ranging from 0.91 to 0.99 across the entire FBW. As demonstrated, the performance characteristics of the developed HDA exceed those of several recently reported unidirectional antenna systems, thus making it a highly desirable option for numerous space-limited wireless applications.

## REFERENCES

- [1] W. Hong, K.-H. Baek, and S. Ko, "Millimeter-wave 5G antennas for smartphones: Overview and experimental demonstration," *IEEE Trans. Antennas Propag.*, vol. 65, no. 12, pp. 6250–6261, Dec. 2017.
- [2] L. Guo, K. W. Leung, and Y. M. Pan, "Compact unidirectional ring dielectric resonator antennas with lateral radiation," *IEEE Trans. Antennas Propag.*, vol. 63, no. 12, pp. 5334–5342, Dec. 2015.
- [3] C. Ding, L. Zhang, J. Dong, and S. Gao, "Characteristic mode inspired single-plate unidirectional antenna using complementary characteristic radiation," *IEEE Trans. Antennas Propag.*, vol. 70, no. 10, pp. 9837–9842, Oct. 2022.
- [4] S. R. Best, "Progress in the design and realization of an electrically small Huygens source," in *Proc. Int. Workshop Antenna Technol. (IWAT)*, Lisbon, Portugal, Mar. 2010, pp. 1–4.
- [5] M.-C. Tang, H. Wang, and R. W. Ziolkowski, "Design and testing of simple, electrically small low-profile, Huygens source antenna with broadside radiation performance," *IEEE Trans. Antennas Propag.*, vol. 64, no. 11, pp. 4607–4617, Nov. 2016.
- [6] W. Lin and R. W. Ziolkowski, "Electrically small, single-substrate Huygens dipole rectenna for ultracompact wireless power transfer applications," *IEEE Trans. Antennas Propag.*, vol. 69, no. 2, pp. 1130–1134, Feb. 2021.
- [7] M.-C. Tang, Z. Wu, T. Shi, and R. W. Ziolkowski, "Dual-band, linearly polarized, electrically small Huygens dipole antennas," *IEEE Trans. Antennas Propag.*, vol. 67, no. 1, pp. 37–47, Jan. 2019.
- [8] P. Jin and R. W. Ziolkowski, "Metamaterial-inspired, electrically small Huygens sources," *IEEE Antennas Wireless Propag. Lett.*, vol. 9, pp. 501–505, May 2010.
- [9] M.-C. Tang, T. Shi, and R. W. Ziolkowski, "A study of 28 GHz, planar, multilayered, electrically small, broadside radiating, Huygens source antennas," *IEEE Trans. Antennas Propag.*, vol. 65, no. 12, pp. 6345–6354, Dec. 2017.
- [10] S.-H. Lee, G. Shin, S. M. Radha, J.-Y. Choi, and I.-J. Yoon, "Low-profile, electrically small planar Huygens source antenna with an endfire radiation characteristic," *IEEE Antennas Wireless Propag. Lett.*, vol. 18, no. 3, pp. 412–416, Mar. 2019.
- [11] W. Lin and R. W. Ziolkowski, "Electrically small, low-profile, Huygens circularly polarized antenna," *IEEE Trans. Antennas Propag.*, vol. 66, no. 2, pp. 636–643, Feb. 2018.
- [12] M.-C. Tang, Z. Wu, T. Shi, H. Zeng, W. Lin, and R. W. Ziolkowski, "Dual-linearly polarized, electrically small, low-profile, broadside radiating, Huygens dipole antenna," *IEEE Trans. Antennas Propag.*, vol. 66, no. 8, pp. 3877–3885, Aug. 2018.
- [13] Z. Wu, M.-C. Tang, T. Shi, and R. W. Ziolkowski, "Two-port, dual-circularly polarized, low-profile broadside-radiating electrically small Huygens dipole antenna," *IEEE Trans. Antennas Propag.*, vol. 69, no. 1, pp. 514–519, Jan. 2021.
- [14] M.-C. Tang, B. Zhou, and R. W. Ziolkowski, "Low-profile, electrically small, Huygens source antenna with pattern-reconfigurability that covers the entire azimuthal plane," *IEEE Trans. Antennas Propag.*, vol. 65, no. 3, pp. 1063–1072, Mar. 2017.
- [15] Z. Wu, M.-C. Tang, M. Li, and R. W. Ziolkowski, "Ultralow-profile, electrically small, pattern-reconfigurable metamaterial-inspired Huygens dipole antenna," *IEEE Trans. Antennas Propag.*, vol. 68, no. 3, pp. 1238–1248, Mar. 2020.
- [16] M.-C. Tang, Z. Wu, T. Shi, and R. W. Ziolkowski, "Electrically small, low-profile, planar, Huygens dipole antenna with quad-polarization diversity," *IEEE Trans. Antennas Propag.*, vol. 66, no. 12, pp. 6772–6780, Dec. 2018.
- [17] M.-C. Tang, T. Shi, and R. W. Ziolkowski, "Electrically small, broadside radiating Huygens source antenna augmented with internal non-Foster elements to increase its bandwidth," *IEEE Antennas Wireless Propag. Lett.*, vol. 16, pp. 712–715, 2016.
- [18] Z. Wu, M.-C. Tang, and R. W. Ziolkowski, "Electrically small, planar, frequency-agile, beam-switchable Huygens dipole antenna," *IEEE Trans. Antennas Propag.*, vol. 69, no. 12, pp. 8271–8281, Dec. 2021.
- [19] P. F. Hu, Y. M. Pan, and B.-J. Hu, "Electrically small, planar, complementary antenna with reconfigurable frequency," *IEEE Trans. Antennas Propag.*, vol. 67, no. 8, pp. 5176–5184, Aug. 2019.
- [20] J. Ouyang, Y. M. Pan, and S. Y. Zheng, "Center-fed unilateral and pattern reconfigurable planar antennas with slotted ground plane," *IEEE Trans. Antennas Propag.*, vol. 66, no. 10, pp. 5139–5149, Oct. 2018.
- [21] K. Wei, Z. Zhang, and Z. Feng, "Design of a wideband horizontally polarized omnidirectional printed loop antenna," *IEEE Antennas Wireless Propag. Lett.*, vol. 11, pp. 49–52, 2012.
- [22] R. W. Ziolkowski, "Low profile, broadside radiating, electrically small Huygens source antennas," *IEEE Access*, vol. 3, pp. 2644–2651, 2015.
- [23] Q. Lin, M.-C. Tang, X. Chen, D. Yi, M. Li, and R. W. Ziolkowski, "Low-profile, electrically small, ultra-wideband antenna enabled with an inductive grid array metasurface," *IEEE Trans. Antennas Propag.*, vol. 70, no. 8, pp. 7152–7157, Jan. 2022.
- [24] C. A. Balanis, *Antenna Theory: Analysis and Design*, 3rd ed. New York, NY, USA: Wiley, 2005.
- [25] W. Lin, R. W. Ziolkowski, and J. Huang, "Electrically small, low-profile, highly efficient, Huygens dipole rectennas for wirelessly powering internet-of-things devices," *IEEE Trans. Antennas Propag.*, vol. 67, no. 6, pp. 3670–3679, Jun. 2019.
- [26] C. Icheln, J. Krogerus, and P. Vainikainen, "Use of balun chokes in small antenna radiation measurements," *IEEE Trans. Instrum. Meas.*, vol. 53, no. 2, pp. 498–506, Apr. 2004.
- [27] *SG128 Multi-Probe Antenna Measurement System*. [Online]. Available: [https://www.mvg-world.com/en/system/files/datasheet\\_sg128\\_bd.pdf](https://www.mvg-world.com/en/system/files/datasheet_sg128_bd.pdf)
- [28] S. Ahdi Rezaeieh, A. Zamani, K. S. Bialkowski, and A. M. Abbosh, "Unidirectional slot-loaded loop antenna with wideband performance and compact size for congestive heart failure detection," *IEEE Trans. Antennas Propag.*, vol. 63, no. 10, pp. 4557–4562, Oct. 2015.
- [29] S. A. Rezaeieh, A. Zamani, and A. M. Abbosh, "3-D Wideband antenna for head-imaging system with performance verification in brain tumor detection," *IEEE Antennas Wireless Propag. Lett.*, vol. 14, pp. 910–914, Apr. 2015.